Effect of Tungsten Addition on Shock Loading Behavior in Ta–W System: A Molecular Dynamics Study

A. Kedharnath, Rajeev Kapoor, and Apu Sarkar

Abstract The effect of tungsten addition to tantalum on spall strength is studied using the molecular dynamics technique. The single crystal configurations with piston plane lying on $(\bar{1}01)$, and $(1\bar{1}1)$ are modeled. The atoms within the piston region are frozen and do not move. The configurations with two tungsten contents of 0 and 10 weight percent tungsten are added as a solvent and equilibrated. The piston velocity is fixed as 1000 m/s and the initial temperature is 0 K. The piston is displaced till 4 nm and stopped which produces a square shock wave moving along $[\bar{1}01]$ and $[1\bar{1}1]$. The configurations are allowed to evolve dynamically using a microcanonical ensemble. The velocity of free surface and spall strength are analyzed for various crystallographic orientations of the single crystal with various tungsten contents. The addition of tungsten to tantalum increased the spall strength due to increased lattice friction provided by the tungsten atoms. Alpha (BCC) to Omega (HCP) phase transformation was observed in $[\bar{1}01]$ oriented single crystal. The addition of tungsten to tantalum resisted this phase transformation.

Keywords Molecular dynamics · Tantalum · Shock loading · Spall strength · Ta–W

1 Introduction

Tantalum and its alloys have profound corrosion resistance properties at high temperatures [1–3]. Tungsten addition to tantalum increases the value of the elastic constants, flow stress, and rate of work hardening [4–7]. Ta–W alloys are proposed alloys for high-temperature reactors and are already been used in containing molten plutonium. Ta–W alloys are used in ballistics and defense materials for their excellent spall strength during shock and high strain rate loading conditions [2, 3, 8]. They also have potential space applications as a coating on base materials and intricate parts to withstand micrometeoroids and debris. Spallation is a ductile fracture

A. Kedharnath (✉) · R. Kapoor · A. Sarkar
Mechanical Metallurgy Division, Bhabha Atomic Research Centre, Mumbai, India

Division of Engineering Sciences, Homi Bhabha National Institute, Mumbai, India

K. Jonnalagadda et al. (eds.), *Advances in Structural Integrity*, Lecture Notes in Mechanical Engineering, https://doi.org/10.1007/978-981-16-8724-2_11

due to the formation and growth of voids which are formed due to the shock wave moving through the metals [9]. Spall strength depends on shock velocity (strain rate), temperature, alloying content, dislocation density, grain boundary types, and grain size [10–12]. Hsiung and Lassila [13] were the first to report phase transformation in BCC tantalum during shock loading deformation. Burakovsky et al. [14] and Haskins et al. [15] used ab initio simulations to explore phases at high pressure and temperature in tantalum. Molecular dynamics (MD) simulations of shock loading on differently oriented tantalum single crystals at various strain rates have been carried out in the last decades [9, 16–19]. Remington et al. [9] performed shock loading simulations on tantalum nanocrystalline configurations and showed that the failure occurred at the interface. The effect of tungsten addition to tantalum on the shock loading behavior of the alloy at various loading orientations is still an active area of research. In this work, the spall strength of pure tantalum and Ta-10 wt.% W oriented along $[\bar{1}01]$ and $[1\bar{1}1]$ directions were studied. The effect of tungsten addition to tantalum was analyzed.

2 Methodology

MD technique is a versatile tool for studying the dynamic evolution of many-body systems and their behavior at the nanoscale level [20, 31]. MD technique can be used for studying mechanical behavior with atomistic defect features such as Frenkel pairs, dislocations, grain boundaries, clusters, segregations, and precipitates [21–24]. MD technique involves solving Newton's equations and updating the atomic positions and velocities ($\boldsymbol{v}$) based on the interatomic potential (E_i) (Eqs. 1–3) [20, 31]. For metallic systems, embedded atom model (EAM) is used for calculating the pairwise part ($\phi(\boldsymbol{r})$) and electronic part ($U \wedge \rho(\boldsymbol{r})$).

$$\boldsymbol{F} = m\boldsymbol{a} = m\frac{d\boldsymbol{v}}{dt} = m\frac{d^2\boldsymbol{r}}{dt^2} \tag{1}$$

$$\boldsymbol{F} = -\nabla E_i \tag{2}$$

$$E_i = U\left(\sum_{j\neq i}\rho(\boldsymbol{r}_{ij})\right) + \frac{1}{2}\sum_{j\neq i}\phi(\boldsymbol{r}_{ij}) \tag{3}$$

$\boldsymbol{F}$ is the force between the atoms of mass m separated by a distance $\boldsymbol{r}_{ij}$. U is the embedding energy for an atom in the electron cloud with the electron transfer function $\rho(\boldsymbol{r})$. Classical MD code implemented through Large-scale Atomic/Molecular Massively Parallel Simulator (LAMMPS) [25] was used and Open Visualization Tool (OVITO) [26] was used for visualization.

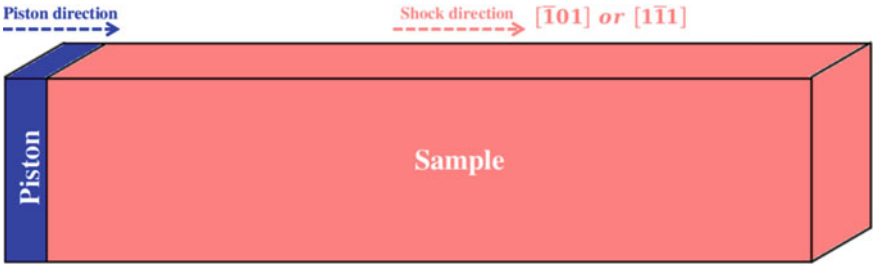

Fig. 1 Schematic of the simulation cell. Piston and its displacement direction are shown in blue color and the sample and the shock wave direction through the sample are shown in red color

Single crystals of tantalum with orientations $\left[\bar{1}01\right]$ and $\left[1\bar{1}1\right]$ along Z direction were modeled using Atomsk [27] and the schematic of the configuration is shown in Fig. 1. The third direction in both the single crystal configurations was $\langle 112 \rangle$. The box dimension of $25 \times 25 \times 100\,\text{nm}^3$ with 3.5 million atoms was chosen. One set of simulations were done on tantalum and the others were done on Ta-10 wt.% W. Ta atoms were randomly replaced/substituted by 10 wt.% (9.858 at.%) tungsten atoms and equilibrated to minimum energy configuration. The configurations were named as per the tungsten content and their orientation, for example, Ta_ $\left[\bar{1}01\right]$ refer to pure tantalum with $\left[\bar{1}01\right]$ along the Z direction and Ta-10W_ $\left[1\bar{1}1\right]$ refer to Ta-10 wt.% tungsten with $\left[1\bar{1}1\right]$ along the Z direction. The piston method of shock loading was used with a constant piston velocity of 1000 m/s. In the piston method, a group of rigid atoms (blue-colored in Fig. 1) is moved at constant velocity to create a perfect square shock wave that travels through the sample (red-colored in Fig. 1). The piston was displaced for 4 picoseconds (ps) moving 4 nm along the Z direction and then stopped. The microcanonical ensemble was used throughout the simulation. The initial temperature of the simulations was maintained near 0 K. The timestep of 0.002 femtoseconds (fs) was used. Periodic boundary conditions were used in X and Y directions and shrink-wrapped in the Z direction. The stress distribution along the Z direction and velocity of the atoms near the free surface was calculated to visualize the attenuation of the wave. The configurations were analyzed using common neighbor analysis (CNA), dislocation extraction algorithm (DXA), and velocity profile. The atoms were colored green for atoms that do not have any structure (other atoms) and brown for HCP atoms; the BCC atoms were removed after CNA. Using DXA, the atoms were removed to visualize dislocations and defect mesh surface generated using voids and defect atoms.

3 Results and Discussion

The stress (σ_{zz}) distribution along Z direction at various timesteps for Ta_ $[\bar{1}01]$ configuration is shown in Fig. 2a. The velocity of the free surface of various configurations is shown in Fig. 2b. The maximum velocity achieved by the free surface is highest in pure tantalum. Tungsten addition increases the lattice friction force which is the reason for the decrease in the peak velocity achieved by the free surface during the shock loading simulation.

Figure 3 gives the spall strength of various configurations. The spall strength is the difference between the minimum and maximum stress experienced by the sample during shock loading simulation. The addition of 10 wt.% tungsten to tantalum

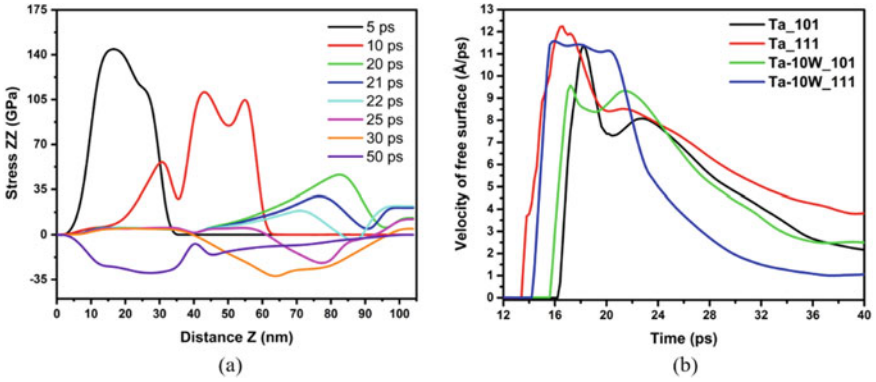

Fig. 2 **a** Stress (σ_{zz}) at various timesteps for Ta_ $[\bar{1}01]$ configuration. **b** The velocity of the free surface of various configurations

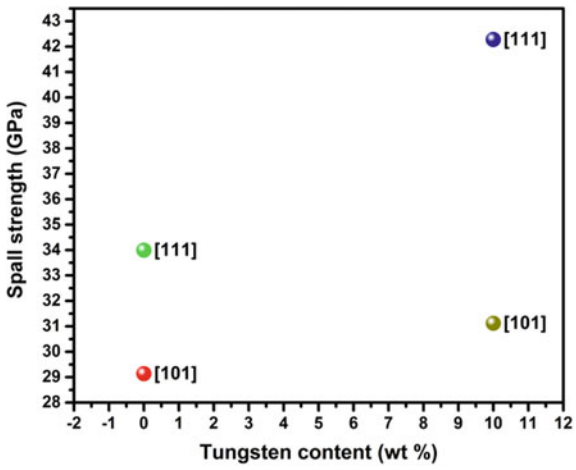

Fig. 3 Spall strength for pure tantalum and Ta-10 W for $[\bar{1}01]$ and $[1\bar{1}1]$ orientations. The colors are used to differentiate the data points

increases the spall strength from 29 to 31 GPa in $\left[\bar{1}01\right]$ orientation and from 34 to 42 GPa in $\left[1\bar{1}1\right]$ orientation.

The spallation events of various configurations are visualized in Fig. 4. The primary spallation was observed near the piston region due to void growth and coalescence caused by the overlap of tensile (returning wave) and compressive waves. The velocity profile showed the velocity of the compression and tensile waves. CNA results showed a phase transformation from BCC (α phase) to HCP (ω phase). DXA results showed the increased dislocation drag in Ta-10 W configurations due to increased lattice Peierls stress by the tungsten atoms. At 104 ps, the dislocations reached the free surface in pure Ta configurations while in Ta-10 W configurations they couldn't and this can be attributed to the dislocations dragging by the tungsten atoms.

Figure 5 shows the phase transformation from BCC $\rightarrow$ HCP in $\left[\bar{1}01\right]$ oriented single crystals. The phase transformation from BCC (α phase) to HCP (ω phase) takes place due to dynamic shear deformation along $\langle 111\rangle$ direction causing changes in stacking sequence in {112} planes [28]. The stacking sequence in {112} BCC planes are ***ABCDEF*** which transform to form omega sequence ***ABED*** [29]. The dissociation of two $\frac{1}{2}\langle 111\rangle$ dislocations into two $\frac{1}{12}\langle 111\rangle$ and one $\frac{1}{3}\langle 111\rangle$ in {112} planes to form the omega phase is energetically favorable as seen in Eq. (4) [30].

$$b^2 > b_1^2 + b_2^2 + b_3^2 \tag{4}$$

The orientation relation between BCC and HCP phases is given by two possible models [13, 30]:

Collapse model: $\{111\}\|\{0001\}\ \langle 110\rangle\|\langle 1120\rangle$

New model: $\{112\}\|\{1100\}\ \langle 111\rangle\|\langle 0001\rangle$ and $\langle 110\rangle\|\langle 1120\rangle$

According to the collapse model, one pair of {111} planes in the BCC phase collapse to form {0001} in HCP phase [13, 29, 30]. In the current $\left[\bar{1}01\right]$ oriented single crystal simulation, the $\{110\}_{bcc}$ planes are parallel to $\{0001\}_{hcp}$ and the $\langle 111\rangle$ directions are parallel to $\langle 11\bar{2}0\rangle$ direction. The new model [13, 30] takes into consideration the stacking sequence in {112} planes and shear in $\langle 111\rangle$ directions. Hsiung et al. [13] showed that Ta-10 W alloy had a higher fraction of HCP phase (transformed from bcc) as compared to pure Ta, but did not explain this. However, the current MD results showed that Ta-10 W had a lower number of atoms in the HCP phase as compared to that of pure Ta. This result could be explained by the increase in the lattice friction with the addition of W to Ta, as the shear modulus of Ta is 69 GPa and that of tungsten is 130 GPa. An increase in lattice friction results in a higher resistance to shear deformation. The fraction of the HCP phase (obtained as fraction of hcp atoms to total number of atoms) are 3.9% for pure Ta and 3.2% for Ta-10 W at 14 ps (snapshot in Fig. 5). At 14 ps, the atomic fractions within the FCC phase are 2.2% for pure Ta and 1.6% for Ta-10 W.

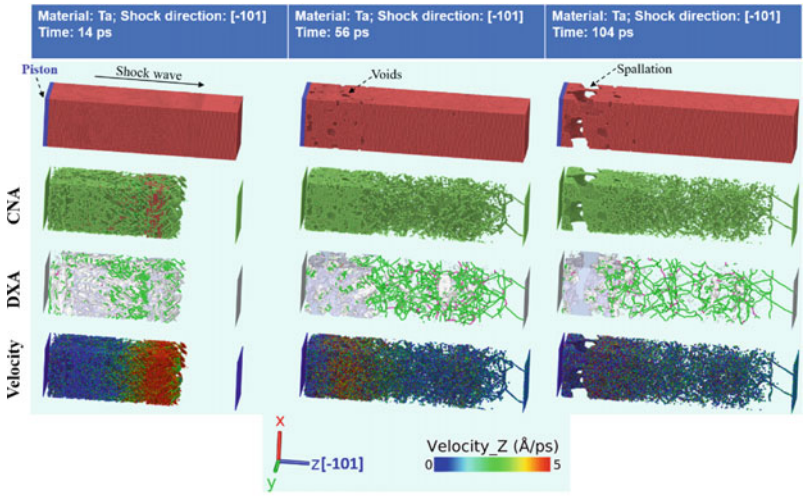

(a)

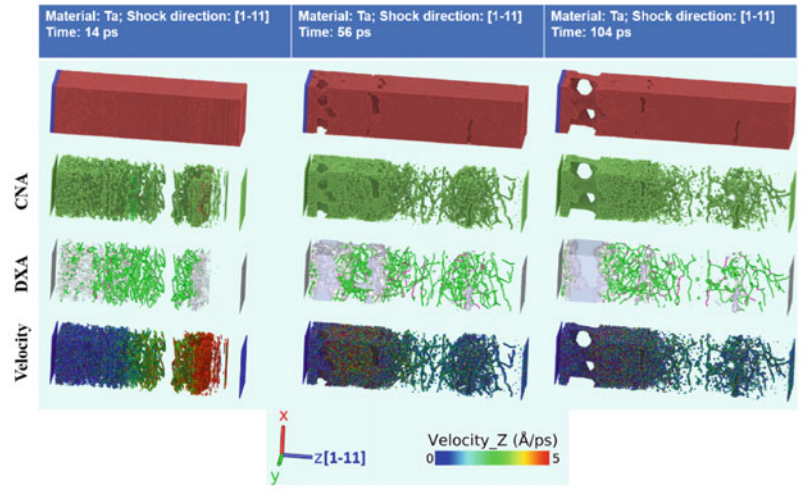

(b)

Fig. 4 Analysis and visualization of various configurations **a** Ta_ $[\bar{1}01]$, **b** Ta_ $[1\bar{1}1]$, **c** Ta-10W_ $[\bar{1}01]$, and **d** Ta-10W_ $[1\bar{1}1]$. The material, shock direction, and timestep are shown at the top, the coordinate axis and velocity scale are shown at the bottom of the figure. In each figure, configurations after piston modeling, CNA, DXA, and velocity profiling along the Z direction are visualized. In the piston model, the blue-colored atoms are modeled as the piston, the brown-colored atoms are tantalum and the yellow-colored atoms are tungsten. After CNA, the BCC atoms are removed, HCP atoms are brown colored and other atoms are green colored. After DXA, the atoms are removed to visualize dislocations and surface mesh. The green-colored dislocations are perfect dislocation and the red-colored dislocations are partial dislocations. After removing the BCC atoms after CNA, the atoms are colored according to the velocity scale

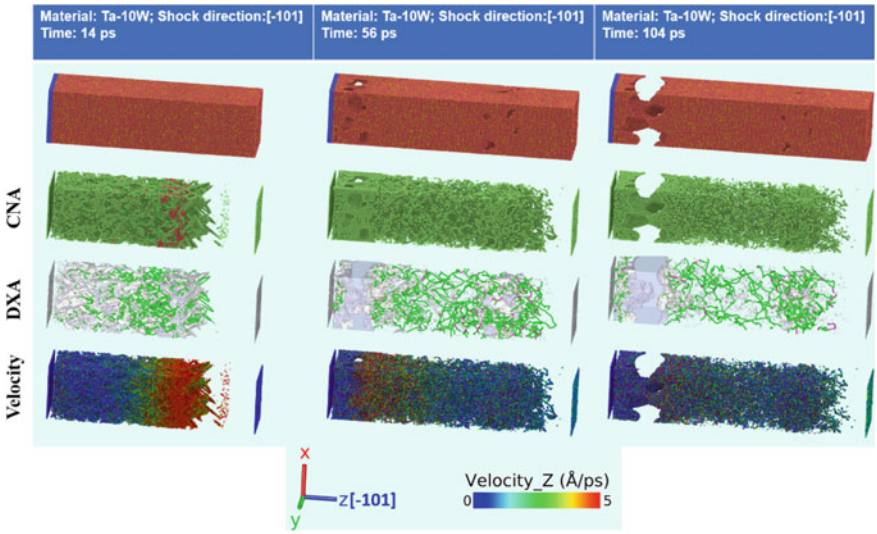

(c)

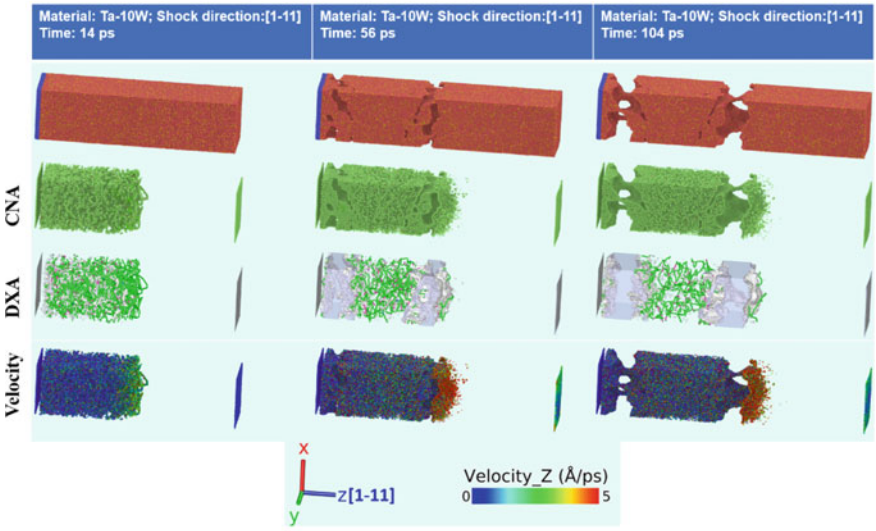

(d)

Fig. 4 (continued)

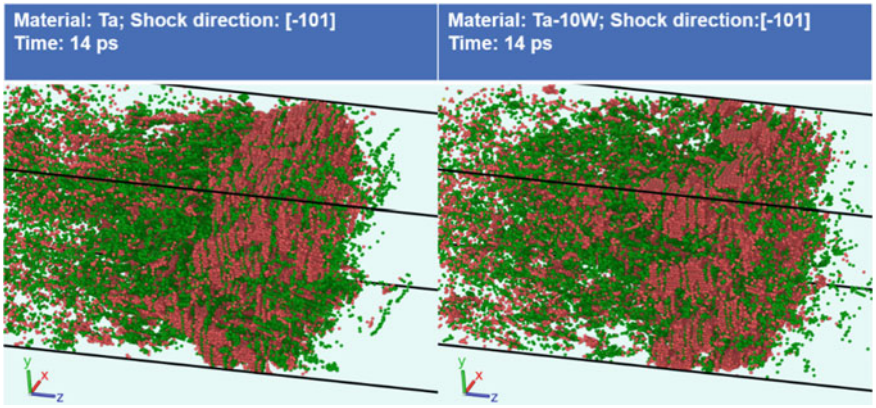

Fig. 5 Phase transformation observed in $[\bar{1}01]$ orientations of Ta and Ta-10 W configurations after CNA. The green-colored atoms are FCC atoms, the brown-colored atoms are HCP atoms and BCC atoms are removed

4 Conclusion

The current MD results and observations on the effect of tungsten addition to tantalum are listed below:

- The spallation event occurred due to the overlap of tensile and compressive waves leading to void formation, growth, and coalescence, and finally ductile fracture.
- Dislocation activity due to the compressive wave got hindered in Ta-10 W due to the increased drag force on the dislocations provided by tungsten atoms.
- Ta-10 W alloy showed a significant increase in spall strength as compared to pure Ta.
- BCC (α phase) $\rightarrow$ HCP (ω phase) transformation was observed for $[\bar{1}01]$ oriented single crystal, but not for the $[1\bar{1}1]$ oriented single crystal. The addition of tungsten reduced the ω phase formation, which was attributed to an increase in lattice friction.

References

1. Köck W, Paschen P (1989) Tantalum-processing, properties and applications. Jom 41:33–39. https://doi.org/10.1007/BF03220360
2. Cardonne SM, Kumar P, Michaluk CA, Schwartz HD (1995) Tantalum and its alloys. Int J Refract Met Hard Mater 13:187–194. https://doi.org/10.1016/0263-4368(95)94023-R
3. Buckman RW Jr (2000) New applications for tantalum and tantalum alloys. JOM 52:40–41
4. Arsenault RJ (1966) An investigation of the mechanism of thermally activated deformation in tantalum and tantalum-base alloys. Acta Metall 14:831–838. https://doi.org/10.1016/0001-6160(66)90003-4

5. Mitchell TE, Raffo PL (1967) Mechanical properties of some tantalum alloys. Can J Phys 45:1047–1062. https://doi.org/10.1139/p67-077
6. Smialek RL, Mitchell TE (1970) Interstitial solution hardening in tantalum single crystals. Philos Mag 22:1105–1127. https://doi.org/10.1080/14786437008226921
7. Anderson CE, Brotzen FR (1982) Elastic constants of tantalum-tungsten alloys. J Appl Phys 53:292–297. https://doi.org/10.1063/1.329929
8. Kothari M, Anand L (1998) Elasto-viscoplastic constitutive equations for polycrystalline metals: Application to tantalum. J Mech Phys Solids 46:51–67. https://doi.org/10.1016/S0022-5096(97)00037-9
9. Remington TP, Hahn EN, Zhao S, Flanagan R, Mertens JCE, Sabbaghianrad S, Langdon TG, Wehrenberg CE, Maddox BR, Swift DC, Remington BA, Chawla N, Meyers MA (2018) Spall strength dependence on grain size and strain rate in tantalum. Acta Mater 158:313–329. https://doi.org/10.1016/j.actamat.2018.07.048
10. Agarwal G, Dongare AM (2017) Atomistic study of shock hugoniot of single crystal Mg. AIP Conf Proc 1793. https://doi.org/10.1063/1.4971592
11. Agarwal G, Dongare AM (2016) Shock wave propagation and spall failure in single crystal Mg at atomic scales. J Appl Phys 119. https://doi.org/10.1063/1.4944942
12. Xiang M, Hu H, Chen J (2013) Spalling and melting in nanocrystalline Pb under shock loading: Molecular dynamics studies. J Appl Phys 113. https://doi.org/10.1063/1.4799388
13. Hsiung L, Lassila D (1998) Shock-induced displacive transformations in Ta and Ta-W alloys. Scr Mater 39:603–609. https://doi.org/10.1016/S1359-6462(98)00203-6
14. Burakovsky L, Chen SP, Preston DL, Belonoshko AB, Rosengren A, Mikhaylushkin AS, Simak SI, Moriarty JA (2010) High-pressure-high-temperature polymorphism in Ta: Resolving an ongoing experimental controversy. Phys Rev Lett 104:1–4. https://doi.org/10.1103/PhysRevLett.104.255702
15. Haskins JB, Moriarty JA, Hood RQ (2012) Polymorphism and melt in high-pressure tantalum. Phys Rev B - Condens Matter Mater Phys 86:18–22. https://doi.org/10.1103/PhysRevB.86.224104
16. An Q, Ravelo R, Germann TC, Han WZ, Luo SN, Tonks DL, Goddard WA (2012) Shock compression and spallation of single crystal tantalum. AIP Conf Proc 1426:1259–1262. https://doi.org/10.1063/1.3686509
17. Hahn EN, Fensin SJ, Germann TC, Gray GT (2018) Orientation dependent spall strength of tantalum single crystals. Acta Mater 159:241–248. https://doi.org/10.1016/j.actamat.2018.07.073
18. Hahn EN, Germann TC, Ravelo R, Hammerberg JE, Meyers MA (2017) On the ultimate tensile strength of tantalum. Acta Mater 126:313–328. https://doi.org/10.1016/j.actamat.2016.12.033
19. Hahn EN, Germann TC, Ravelo RJ, Hammerberg JE, Meyers MA (2017) Non-equilibrium molecular dynamics simulations of spall in single crystal tantalum. AIP Conf Proc 1793. https://doi.org/10.1063/1.4971594
20. Frenkel D, Smit B (2002) Understanding Molecular Simulation From Algorithms to Applications, Vol. 2. Academic Press
21. Kedharnath A, Kapoor R, Sarkar A (2019) Atomistic simulation of interaction of collision cascade with different types of grain boundaries in α-Fe. J Nucl Mater 523:444–457 . https://doi.org/10.1016/j.jnucmat.2019.06.021
22. Kedharnath A, Panwar AS, Kapoor R (2017) Molecular dynamics simulation of the interaction of a nano-scale crack with grain boundaries in α-Fe. Comput Mater Sci 137:85–99. https://doi.org/10.1016/j.commatsci.2017.05.026
23. Singh D, Parashar A, Kedharnath A, Kapoor R, Sarkar A (2019) Molecular dynamics-based simulations to study crack tip interaction with symmetrical and asymmetrical tilt grain boundaries in Zr. J Nucl Mater 526. https://doi.org/10.1016/j.jnucmat.2019.151739
24. Singh D, Parashar A, Kedharnath A, Kapoor R, Sarkar A (2019) Effect of symmetrical and asymmetrical tilt grain boundaries on the tensile deformation of zirconium bicrystals: a MD-based study. J Mater Sci 54:3082–3095. https://doi.org/10.1007/s10853-018-3032-7

25. Plimpton S (1995) Fast parallel algorithms for short-range molecular dynamics. J Comput Phys 117:1–19. https://doi.org/10.1006/jcph.1995.1039
26. Stukowski A (2010) Visualization and analysis of atomistic simulation data with OVITO-the Open Visualization Tool. Model Simul Mater Sci Eng 18. https://doi.org/10.1088/0965-0393/18/1/015012
27. Hirel P (2015) Atomsk: A tool for manipulating and converting atomic data files. Comput Phys Commun 197:212–219. https://doi.org/10.1016/j.cpc.2015.07.012
28. Lu CH, Hahn EN, Remington BA, Maddox BR, Bringa EM, Meyers MA (2015) Phase Transformation in Tantalum under Extreme Laser Deformation. Sci Rep 5:1–8. https://doi.org/10.1038/srep15064
29. Hsiung LM, Lassila DH (2000) Shock-induced deformation twinning and omega transformation in tantalum and tantalum-tungsten alloys. Acta Mater 48:4851–4865. https://doi.org/10.1016/S1359-6454(00)00287-1
30. Hsiung LL (2010) Shock-induced phase transformation in tantalum. J Phys Condens Matter 22. https://doi.org/10.1088/0953-8984/22/38/385702
31. Kedharnath A, Kapoor R, Sarkar A (2021) Classical molecular dynamics simulations of the deformation of metals under uniaxial monotonic loading: a review. Comput Struct 254:106614. https://doi.org/10.1016/j.compstruc.2021.106614